Progress In Electromagnetics Research C, Vol. 123, 167–179, 2022

Design and Analysis of a Novel Mechanical Variable Flux Interior Permanent Magnet Synchronous Motor

Jianwei Liang, Dabin Liu*, Yun Gao, Hongwei Yuan, and Xiping Liu

Abstract—In this paper, a novel mechanical variable flux interior permanent magnet synchronous motor (MVF-IPMSM) is proposed. Based on the basic topology and operating principle of MVF-IPMSM, the effect of the special PMs structure in the new rotor topology on the air gap magnetic field and the design of the mechanical magnetic adjustment device of the proposed motor are analyzed, in which the finite element analysis (FEA) method is adopted. The electromagnetic characteristics of the MVF-IPMSM are analyzed including internal magnetic field distribution, air gap flux density, and torque characteristics. Furthermore, the ability of magnetic field regulation is also analyzed which can be reflected by the torque-speed and power-speed envelopes. Finally, a prototype is manufactured and tested. The measured results are compared with the FEA results, and the prototype experiments verify the effectiveness and feasibility of the design of the proposed MVF-IPMSM.

1. INTRODUCTION

Interior permanent magnet synchronous motors (IPMSMs) are widely used in many filed such as home appliances and electric vehicles due to their simple structure and operational reliability with the advantages of high efficiency, high power factor, and high torque density [1, 2]. However, the common problem of IPMSM is that the internal magnetic field is difficult to adjust and cannot be solved in a regular way which has raised a lot of consideration for many scholars and experts, and thus a variety of topologies of IPMSM named variable flux motors (VFM) have been proposed. To adjust the internal magnetic field which is limited by bus voltage, a series of flux weakening control strategies are formed that inject negative d-axis current which can weaken the air gap flux density by controlling the armature current to achieve a wider constant power speed range. But meanwhile, excessive demagnetization current will cause additional copper loss which will result in lower efficiency [3–5]. Therefore, novel topologies and flux-adjusting mechanisms of the VFM have been proposed in recent years, and the VFM not only has the advantages of the traditional permanent magnet (PM) motor but also can effectively adjust its internal magnetic field [6, 7]. In the current state of research, Mechanical Variable-Flux Motor (MVFM) [7–18] has attracted increasing attention of experts and scholars.

The MVFM mentioned above has no excitation winding which means less power loss, and its air gap flux density can be adjusted according to the operating state, which can greatly reduce the control difficulty of the drive system [11]. At present, MVFM can be divided into radial type [7–13] and axial type [10, 14] according to the direction of its air gap flux. In [7], an axially MVFM is proposed in which the special three-segment split rotor structure design can make the flux short-circuit or in the maximum state when the magnetic poles are aligned, and the middle rotor can rotate to realize flux adjusting. The motor in [8] adopted centrifugal force to drive the segmented rotor to rotate around its axis to realize online flux adjusting. In [9], online flux adjusting can be achieved by adjusting the leakage flux

Received 8 July 2022, Accepted 16 August 2022, Scheduled 29 August 2022

* Corresponding author: Dabin Liu (liudb211@163.com).

The authors are with the Department of Electrical Engineering and Automation, Jiangxi University of Science and Technology, Ganzhou, China.

using a moving slider, to enhance the flux weakening ability of the motor when it runs at high speed. A novel MVFM with a staggered rotor is proposed in [10], and staggered rotors can change the flux generated by coils under the structure of slotted stator and non-slotted stator.

In this paper, a new topology of variable flux IPMSM (MVF-IPMSM) is proposed, which has the function of online flux-adjusting due to the mechanical magnetic adjustment device. The slider of the mechanical magnetic adjustment device is driven by centrifugal force to rotate the cylindrical permanent magnets (CPMs) at different speeds around the axis to different angles, which is equivalent to changing the magnetizing direction of the PMs, thereby adjusting the air gap flux density to achieve a wider speed range. In [12], an MVFM with rotating magnetic poles (MVFM-RMPs) has a problem that when the rotation angle of the CPMs is too large, the leakage flux is uncontrollable, and the waveform of air gap flux density is seriously distorted, which cannot meet the normal operation, and the MVF-IPMSM can solve this problem suitably.

2. MOTOR TOPOLOGY AND WORKING PRINCIPLE

The proposed MVF-IPMSM is composed of double-layer interior PMs and a mechanical magnetic adjustment device, as shown in Fig. 1. The mechanical magnetic adjustment device is attached to the rotor, and the CPMs are rigidly connected through a support rod. A gap is reserved between the CPMs and the rotor which allows the CPMs to rotate.

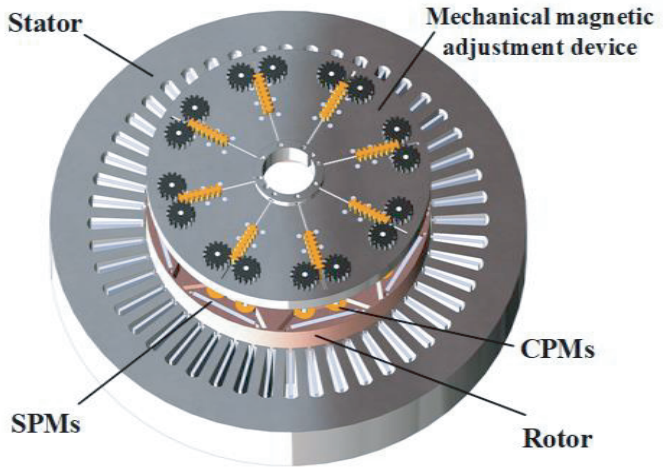

Figure 1. 3D Drawing of motor structure.

The interior PMs of the MVF-IPMSM include two CPMs and one square permanent magnet (SPM) per pole. Both the mechanical magnetic adjustment device and PMs have strict size requirements to fit and reduce friction when rotating, and the unique rotor topology can not only adjust the air gap flux density but also greatly weaken the adverse effects caused by the severe distortion of the waveform of air gap flux density. The MVF-IPMSM can flexibly adjust its internal magnetic field without extra excitation or pulse current which means less copper loss.

When the speed of the proposed MVF-IPMSM varies within a certain range, the mechanical magnetic adjustment device can be dynamic to adjust the rotation angle of the CPMs which is defined as θ with the motor operating state, and increase or decrease the leakage flux of the MVF-IPMSM in real-time, thereby adjusting the air gap flux density of the motor. When the motor runs below the rated speed (1500 rpm), the mechanical magnetic adjustment device does not act, and the motor operates in the constant torque region. But when the motor runs above the rated speed, the mechanical magnetic adjustment device starts to work, and the CPMs start to rotate which means that the rotation angle θ gradually increases, and the leakage flux also increases. When the motor runs to the system threshold and above, the leakage flux is the largest, and the mechanical magnetic adjustment device is no longer working. In MVF-IPMSM, SPMs are the main contributors to air gap flux density, while CPMs mainly

regulate leakage flux.

Based on the analysis above, the proposed MVF-IPMSM can flexibly adjust the internal magnetic field under the function of the mechanical magnetic adjustment device, which means that the leakage flux can be adjusted, and the flux can be changed thereby widening its speed regulation range.

2.1. Stator and Rotor Topology

As shown in Fig. 2, the rotor structure of MVF-IPMSM in Fig. 2(c) evolved from MVFM-RMP in Fig. 2(a). And the MVF-IPMSM adopts double layers of PMs which contain 1 SPM and 2 CPMs on each pole in the rotor which draws on the structure of prius 2017, shown in Fig. 2(b). Due to the particularity of the flux barriers design, the proposed motor has a high salient rate and output torque, and under the function of a mechanical magnetic adjustment device, the CPMs rotate around the axis and automatically change the self-leakage flux of PMs and flux leakage between adjacent poles to achieve variable flux effect.

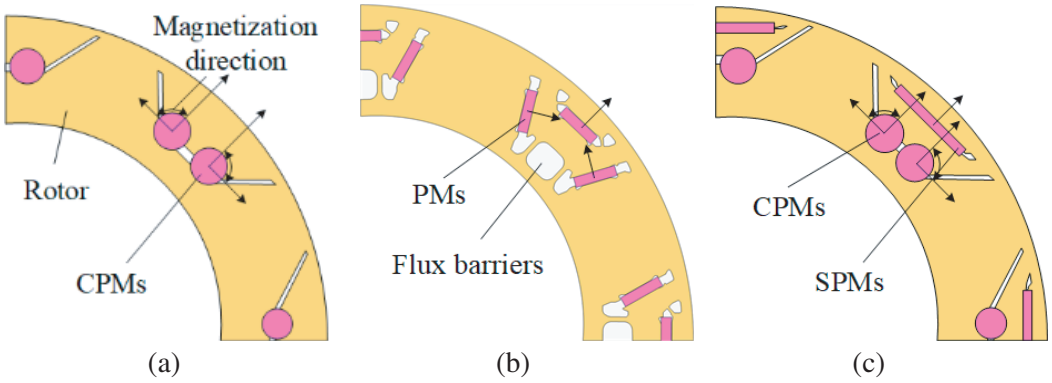

Figure 2. Topology of stator and rotor. (a) MVFM-RMP. (b) Prius 2017. (c) MVF-IPMSM.

2.2. Mechanical Magnetic Adjustment Device Design

The mechanical magnetic adjustment device is composed of a turntable, gears, connecting rods, sliders, and springs as shown in Fig. 3. The device is composed of the main turntable and a secondary turntable, and the connecting rod is rigidly connected with the gear, runs through the main turntable and the secondary turntable, and rotates coaxially and synchronously with the rotor.

The mechanical magnetic adjustment device uses a centrifugal slider as the driving element for the rotation of the gear, and then the gear is moved radially through the meshing transmission between

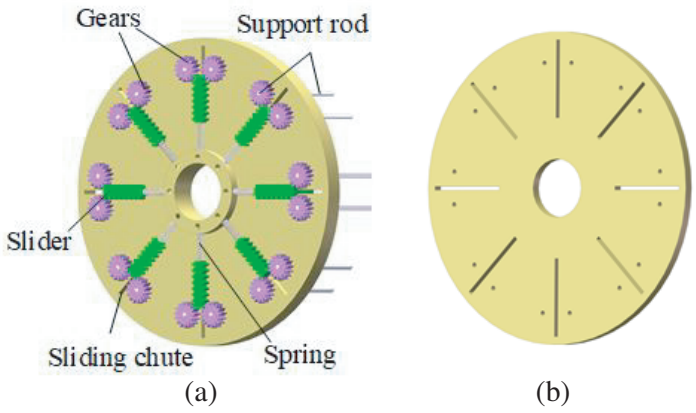

Figure 3. Mechanical magnetic adjustment device. (a) Main turntable. (b) Secondary turntable.

the sliders and the gear. After that, the CPMs are driven to rotate around the axis. A sliding chute is set up in the turntable, and the spring is in the chute which is connected to one end of the slider. The sliding chute can not only ensure that the slider has good stability during the operation of the motor, but also flexibly generate steady displacement under the action of centrifugal force. The contact surface between the chute and the slider needs to be specially treated to reduce sliding friction, and the 8-pole device can run synchronously.

2.3. The Operating Status of the Motor

The mechanical magnetic adjustment device rotates coaxially with the rotor and can drive the CPMs to rotate around the axis, thereby changing the leakage flux. The operating states of the motor can be divided into three statuses as shown in Fig. 4.

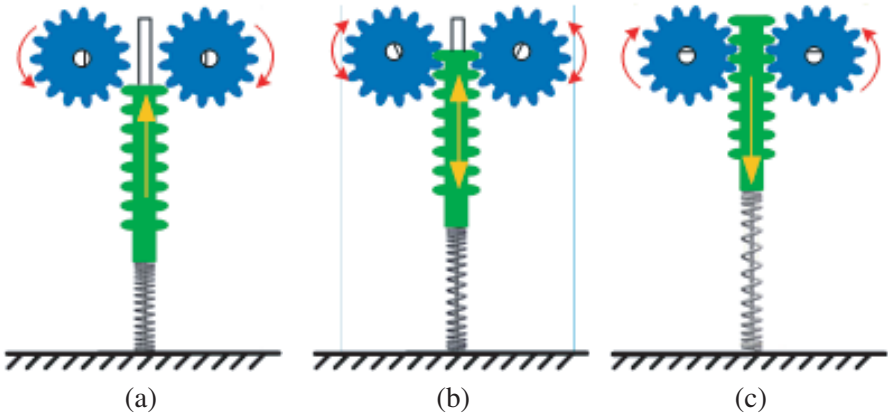

Figure 4. Operation status of device. (a) Initial. (b) Changeable. (c) Limited.

In this design of the MVF-IPMSM, when the motor runs at the rated speed (1500 rpm) and below, the spring tension is less than or equal to the centrifugal force of the slider; the slider is always kept at the bottom; the gear just meshes with the slider; and the mechanical magnetic adjustment device does not work as shown in Fig. 4(a), which is the initial status. When the motor runs above the rated speed, with the running speed varying within a certain range, the radial deformation of the spring causes the slider to push the gear and make the CPMs rotate, which is equivalent to changing the magnetization direction of the PMs. At this time, it the variable flux state, as shown in Fig. 4(b). When the motor speed exceeds the system threshold (3000 rpm) of the mechanical magnetic adjustment device, the slider is at the top of the chute and no longer operates; the rotation angle θ of the CPMs around the axis reaches the maximum value of 90° as shown in Fig. 4(c) which is the limited status; and the motor begins to run in the flux weakening region.

3. ANALYSIS OF AIR GAP MAGNETIC FIELD AND THE MECHANICAL MAGNETIC ADJUSTMENT DEVICE

3.1. Air Gap Magnetic Field Analysis

The SPM and CPMs of each pole of the MVF-IPMSM are parallel magnetized. When the MVF-IPMSM runs at the rated speed and below, the magnetizing directions of the SPMs and CPMs are all radially towards the air gap; when the MVF-IPMSM runs at the rated speed and above, under the function of the mechanical magnetic adjustment device, the CPMs rotate which means that the magnetic circuit and the air gap magnetic field distribution are changed in the meanwhile.

The composite PMs flux linkage vector ψ_f is generated by each PM flux linkage vector, as shown in Fig. 5, where θ is the rotation angle of the CPMs around the axis. The composite PM flux linkage

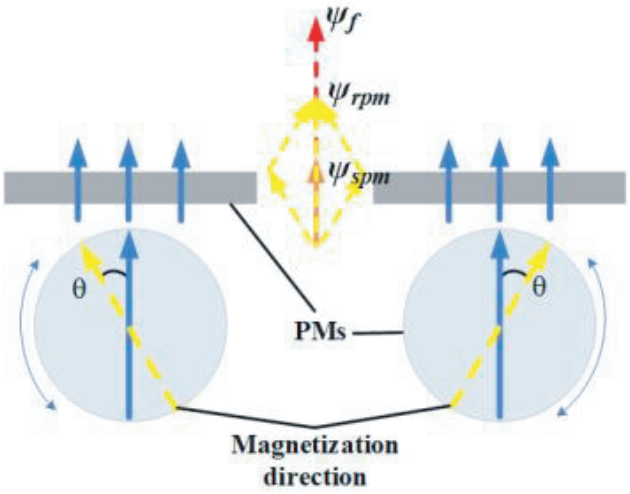

Figure 5. Vector diagram of air gap magnetic field.

vector ψ_f is defined as:

$$\psi_f = \psi_{cpm} + \psi_{spm} \tag{1}$$

where ψ_f is the composite PMs flux linkage, ψ_{cpm} the composite CPMs flux linkage, and ψ_{spm} the composite SPMs flux linkage. The d-q axis mathematical model of the PMSM is established when operating in the flux weakening region based on: (1) the phase winding resistance is ignored; (2) the hysteresis loss is ignored; and (3) the stator armature current is all the d-axis current component. The ideal maximum speed $n_{\max}$ of the PMSM can be deduced as:

$$n_{\max} = \frac{60U_{\max}}{2\pi p\psi_f - L_d I_{\max}} \tag{2}$$

in which $U_{\max}$ is the maximum allowable voltage of the inverter, $I_{\max}$ the maximum allowable current of the inverter, p the pole pairs, and L_d the d-axis inductance. To increase the maximum speed $n_{\max}$ of the motor, we can reduce the composite PMs flux linkage ψ_f or increase L_d. Under the action of the mechanical magnetic adjustment device, the rotation angle θ of the CPMs increases, and ψ_{rpm} decreases accordingly. Then, it can be known that the composite PMs flux linkage ψ_f decreases, and $n_{\max}$ increases accordingly, which can realize a wide speed range.

3.2. Design of the Mechanical Magnetic Adjustment Device

To precisely rotate the CPMs to the desired angle, the mechanical magnetic adjustment device needs to be carefully designed which has very strict size requirements.

The dynamic analysis of the mechanical magnetic adjustment device is necessary, and the force analysis diagram is shown in Fig. 6, where x represents the slider displacement, F_e the spring tension, F_f the friction, and F_c the centrifugal force. It can be derived that the centrifugal force on the slider is:

$$F_c = m\omega^2(r + x + \frac{l}{2}) \tag{3}$$

The spring tension on the slider is:

$$F_e = Kx \tag{4}$$

In addition, the electromagnetic force among the PMs, rotor, and gravity G of the slider itself exists which can be negligible compared with the centrifugal force F_c. At the same time, there is also sliding friction F_f between the slider and the turntable and between the PMs and the slots, but the friction force can be reduced by special treatment of the contact surface to the lowest, so the differential equation for the slider displacement x is:

$$m\frac{dx^2}{dt^2} = F_c - F_e \tag{5}$$

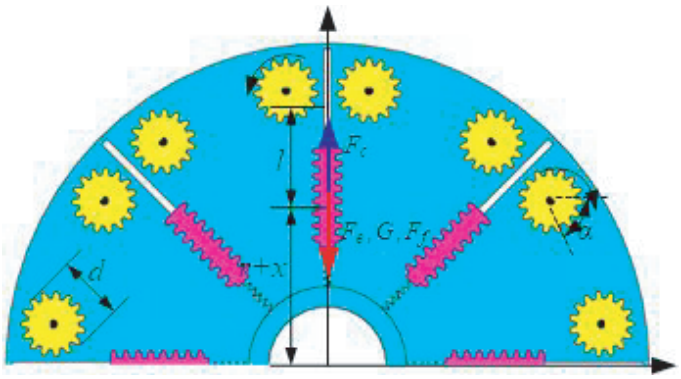

Figure 6. Stress analysis of the mechanical magnetic adjustment device.

The relationship between the x displacement and rotation angle θ of the CPMs is:

$$x = \frac{\theta}{360} d\pi \tag{6}$$

Based on the above analysis, the mechanical magnetic adjustment device is designed, and the main parameters of the mechanical magnetic adjustment device are shown in Table 1.

Table 1. Main parameters of the mechanical magnetic adjustment device.

Parameters	Units	Value
Slider weight m	kg	0.2
Slider length l	mm	25
Chute length	mm	36.8
Initial height of slider r	mm	25
Spring constant K	N/mm	2.5
Gear diameter d	mm	15

4. FINITE ELEMENT ANALYSIS OF ELECTROMAGNETIC CHARACTERISTICS

To fairly evaluate the performance of the MVF-IPMSM, MVFM-RMP is selected as a comparison object, in which PMs with the same material and equal volumes are adopted in the rotors as shown in Table 2. In the comparative analysis, the design variables were set to be consistent, and the electromagnetic characteristics such as the magnetic field distribution and air gap flux density of the two motors at different rotation angle θ were further analyzed. The torque-speed characteristics and power-speed

Table 2. Volume of PMs per pole of two motors.

Parameters	Units	MVF-RMP	MVF-IPMSM
Diameter of CPMs	mm	13.2	10.6
Width of SPMs	mm	N/A	39
Thickness of SPMs	mm	N/A	25
Length	mm	4	40
Volume of PMs per pole	cm^3	10.96	10.96

characteristics of the motor are also analyzed to verify the effectiveness of the mechanical magnetic adjustment device for wide-range speed regulation.

4.1. Magnetic Field Distribution

Figure 7 shows the distribution of flux lines and the flux density of the MFVM-RMP and MVF-IPMSM when the CPMs rotate around the axis with $\theta = 0°$ and $\theta = 45°$, respectively. It can be seen from Fig. 7 that the magnetization direction of the CPMs is shifted by 45° from the initial magnetization direction in Fig. 7(a). And the flux lines inside the motor are relatively sparse when $\theta = 45°$, as shown in Fig. 7(b), due to the increasing leakage flux which weakens the main magnetic field at the meanwhile. It reflects that both MVFM-RMP and MVF-IPMSM can adjust the rotation angle θ of the CPMs at different speeds by the mechanical magnetic adjustment device and then adjust the internal magnetic field of the motor.

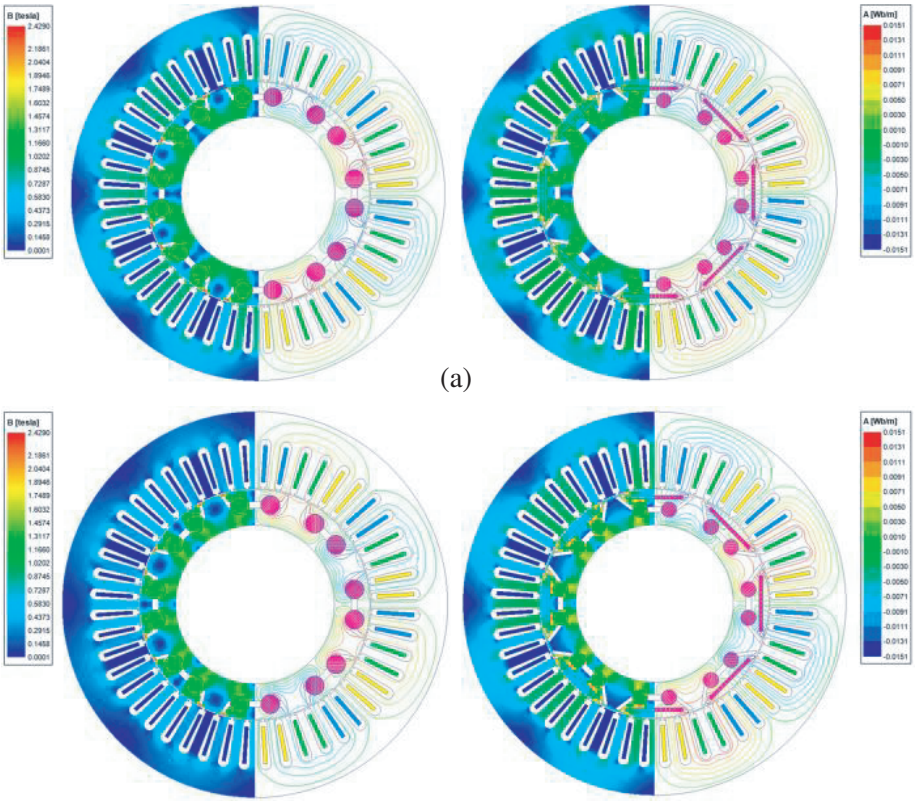

Figure 7. Flux lines and flux distribution of the two motors at different rotation angle. (a) $\theta = 0°$. (b) $\theta = 45°$.

4.2. Flux Linkage Analysis

The analysis of the flux linkage can verify the effectiveness of the mechanical magnetic adjustment device to a certain extent. And the flux linkage under different rotation angles θ of the mechanical magnetic adjustment device is analyzed, and the finite element analysis results are shown in Fig. 8. When the rotation angle of MVFM-RMP reaches 75°, the flux linkage is close to 0, and the MVFM-RMP cannot operate normally. However, when the rotation angle θ of the MVF-IPMSM varies from 0° to 90°, the flux linkage is also changed, and the motor can still run normally. When rotation angle $\theta = 90°$, the speed regulation range of the MVF-IPMSM is wider. The finite element results verify the effectiveness of the mechanical magnetic adjustment device.

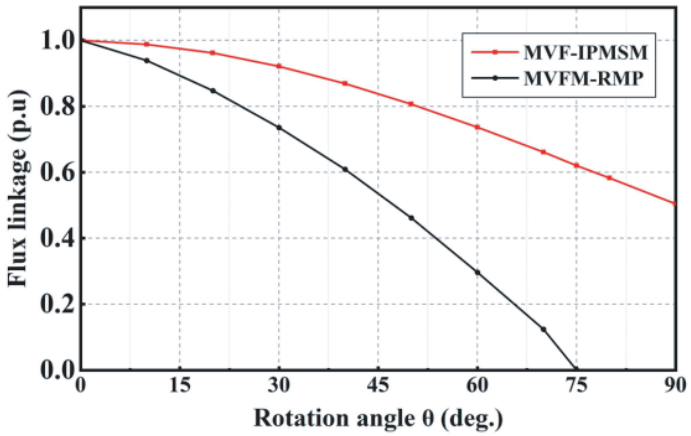

Figure 8. Flux linkage characteristic.

4.3. Air Gap Flux Density

The air gap flux density reflects the output capability of power and torque of PMSM, and the finite element analysis (FEA) method is adopted to calculate the air gap flux density of the two motors. As shown in Fig. 9(a), when the rotation angle θ of the CPMs is 0°, the maximum air gap flux density of the MVFM-RPM is 0.653 T, which can meet the expected operating requirements of the motor. With the increase of the rotation angle θ, the waveform of the air gap flux density distortion begins to occur, and the waveform of the air gap flux density is seriously distorted when the rotation angle $\theta = 60°$. The degree of waveform distortion is further aggravated when the rotation angle θ is greater than 60°.

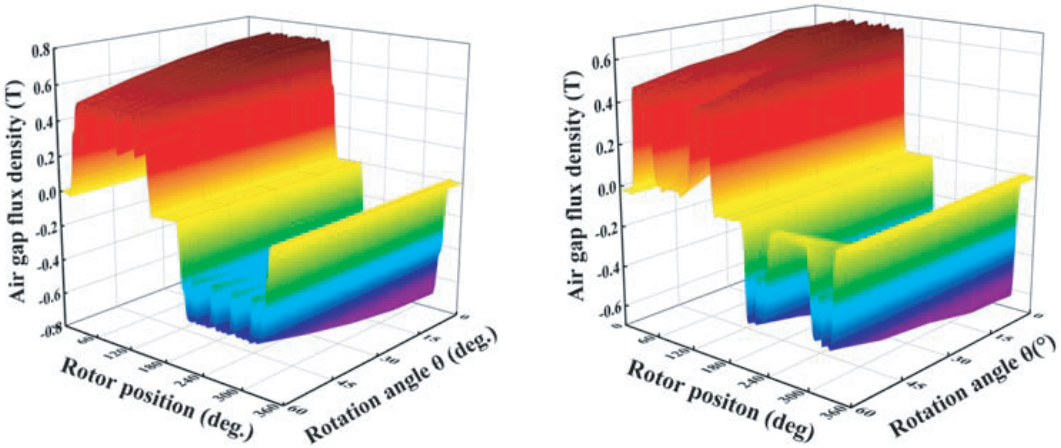

(a) (b)

Figure 9. Air gap flux density distribution. (a) MVFM-RMP. (b) MVF-IPMSM.

As shown in Fig. 9(b), the maximum air gap flux density of VLF-IPMSM is 0.747 T, which improves the utilization rate of CPMs compared with the MVFM-RPM, and as the rotation angle θ increases, the air gap magnetic field is weakened which will result in an obvious effect that the waveform distortion is reduced.

The amplitude of air gap flux density is shown in Table 3. As the rotation angle increases, the amplitude of air gap flux density of the two motors decreases continuously, and finally the waveform of the air gap flux density of the MVFM-RMP is seriously distorted compared with the MVF-IPMSM, which reflects the superiority of the special PMs structure.

Table 3. Amplitude of the air gap flux density.

Rotation Angle	Amplitude of the air gap flux density (T)	
	MVFM-RMP	MVF-IPMSM
0°	0.653	0.747
15°	0.605	0.708
30°	0.501	0.662
45°	0.279	0.601
60°	0.189	0.537

4.4. Torque Performance

The torque characteristics of the two motors at different current angles are shown in Fig. 10(a). The maximum torque current angle of the MVFM-RMP motor is 34.5 deg, and the maximum torque current angle of the MVF-IPMSM is 30.0 deg. Fig. 10(b) shows the relationship between the output torque and rotation angle of the mechanical magnetic control device, in which the torque of MVFM-RMP is decreased by 85.1%, while the output torque of MVF-IPMSM is decreased by only 40.5% which has a better output torque performance.

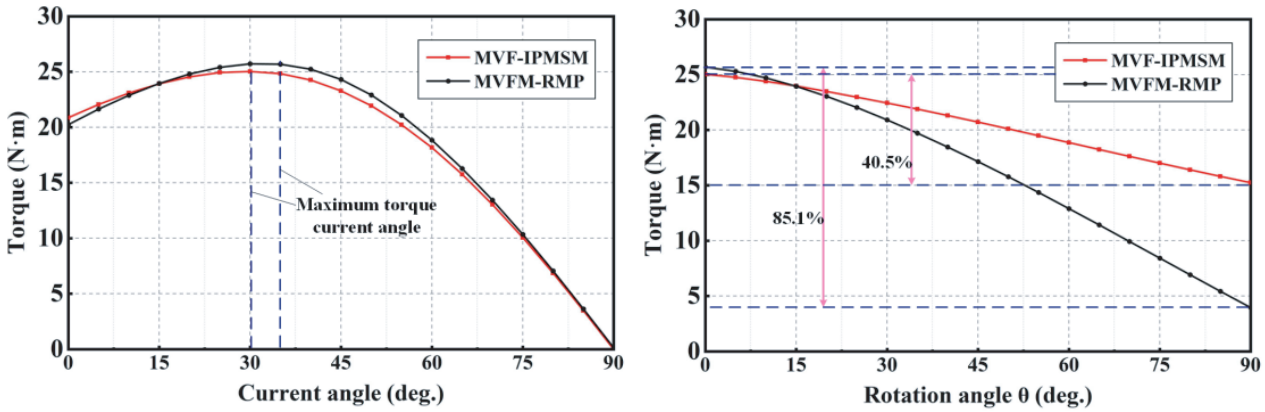

Figure 10. Torque characteristic. (a) Output torque under different current angle conditions. (b) Output torque under different rotation angle conditions.

4.5. Torque-Speed and Power-Speed Envelopes

In the MVF-IPMSM, the rotation angle θ of the mechanical magnetic adjustment device is $0° \sim 90°$, which means that the maximum rotation angle θ of the CPMs is 90°. The torque-speed characteristics and power-speed characteristics are shown in Fig. 11 and Fig. 12. When the motor runs at the base speed and below, the CPMs do not rotate, and its output torque is 25 N m; when the motor runs between the rated speed and twice the rated speed, the rotation angle θ is within the range of $0° \sim 90°$. When the motor runs above 3000 rpm, the rotation angle θ of the device reaches the maximum value of 90° and does not change with the increase of the rotation speed.

In the FEA simulation results, the maximum speed of the proposed motor can reach 10000 rpm, which means that the motor can effectively adjust the magnetic field due to the function of the mechanical magnetic adjustment device and achieve a wide speed range. The magnetic field modulation region is marked in Fig. 11 and Fig. 12.

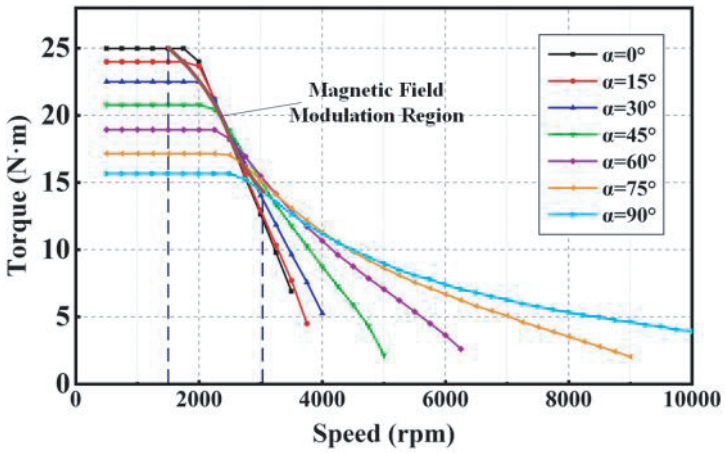

Figure 11. Torque-speed envolopes.

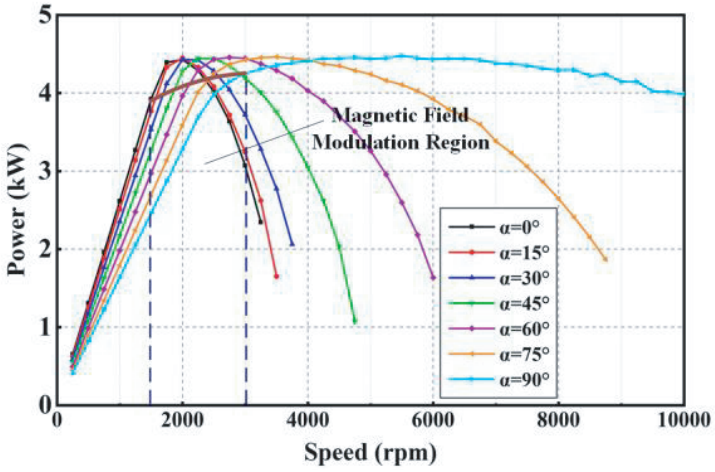

Figure 12. Power-speed envelopes.

5. PROTOTYPE EXPERIMENT AND ANALYSIS

To verify the rationality of the design of the MVF-IPMSM and for the purpose of improving the output torque and widening the speed range, the rotor topology of the MVF-IPMSM is optimized by NSGA-II optimization algorithms, and a prototype is manufactured and tested. The components of the prototype are shown in Fig. 13.

(a) (b)

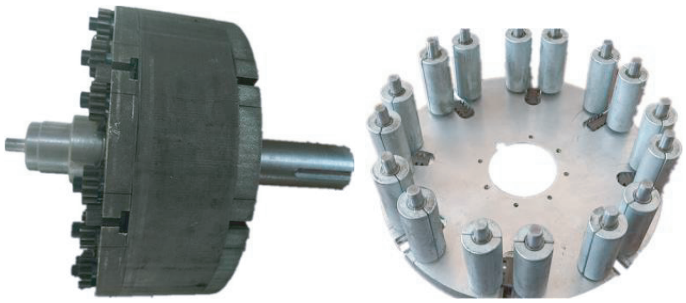

(c) (d)

Figure 13. Prototype. (a) Mechanical magnetic adjustment device. (b) Rotor. (c) Assembly. (d) CPMs.

The no-load back EMF test was carried out on the prototype at 1500 rpm to verify the effectiveness of the proposed MVF-IPMSM. When the motor works at the speed of 1500 rpm, the magnetic adjustment device does not work at this time, and the rotation angle θ is 0°. The no-load back EMF waveform of the FEA result and measured are shown in Fig. 14. The amplitude of no-load back EMF

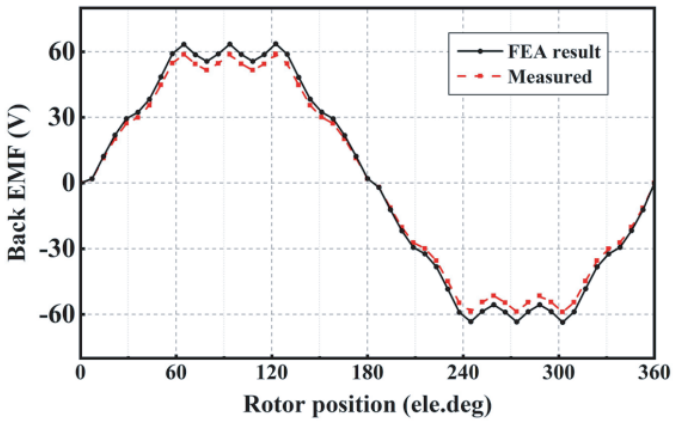

Figure 14. No-load back EMF at the speed of 1500 rpm.

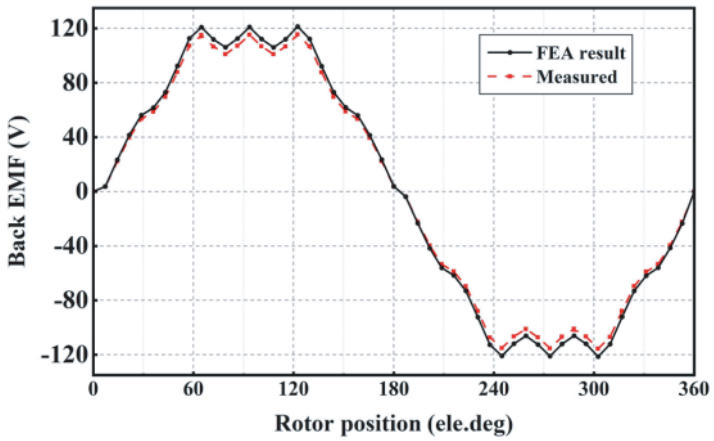

Figure 15. No-load back EMF at the speed of 3000 rpm without the magnetic adjustment device.

of the FEA result is 64.1 V; the amplitudes of no-load back EMF of the prototype measured result is 62 V; the error rate is 3.3% which is within the allowable and reasonable range. It can be seen from the result that the two waveforms have a high consistency, which shows the rationality of the prototype design.

When rotation speed exceeds the threshold value of the magnetic adjustment device (3000 rpm), the rotation angle θ is 90°. The no-load back EMF waveforms of the prototype with and without the magnetic adjustment device were measured respectively, as shown in Fig. 15 and Fig. 16. The prototype was tested without the magnetic adjustment device. The amplitude of the no-load back EMF waveform was 116 V; the FEA result was 120 V; and the error rate is 2.5% which is also within the allowable and reasonable range. Then, the prototype was tested with the magnetic adjustment device. The FEA result and measured results are 50.6 V and 50.2 V, respectively, which show the rationality of the rotor structure design and also verify the effectiveness of the magnetic adjustment device.

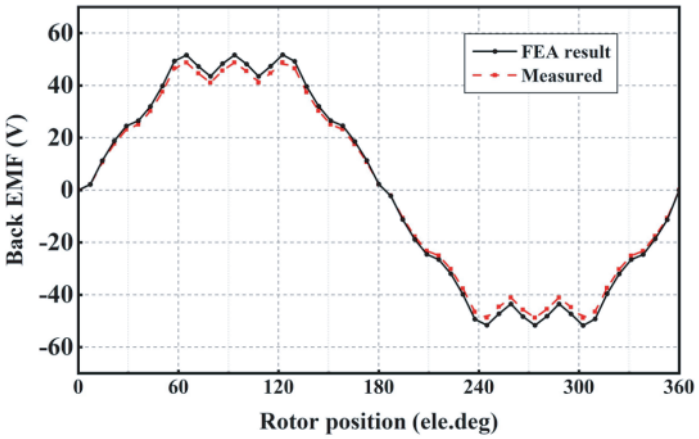

Figure 16. No-load back EMF at the speed of 3000 rpm with the magnetic adjustment device.

6. CONCLUSION

In this paper, a novel mechanical variable flux interior permanent magnet synchronous motor (MVF-IPMSM) is proposed. The magnetic field distribution and electromagnetic characteristics of the proposed motor are analyzed through the FEA method, and a prototype is manufactured to verify the feasibility of the design. The following conclusions are obtained:

(1) The magnetic adjustment device can make the CPMs rotate around the axis correspondingly with the change of the motor speed and control the flux to change, which can effectively widen the speed regulation range without additional control strategies and has high reliability.

(2) The rotor structure of double-layered PMs can greatly reduce the degree of air gap magnetic field distortion caused by excessive rotation angle which can improve the reliability of operation.

ACKNOWLEDGMENT

This work was supported in part by the National Natural Science Foundation of China under grant No. 51767009, in part by the Plan Project of Jiangxi Province of P. R. China under grant No. 20181BAB206035.

REFERENCES

1. Pellegrino, G., A. Vacate, P. Guglielmo, and B. Boazzo, "Performance comparison between surface-mounted and interior PM motor drives for electric vehicle application," *IEEE Transactions on Industrial Electronics*, Vol. 59, No. 2, 803–811, Feb. 2012.

2. Cheng, M., P. Han, and W. Hua, "General airgap field modulation theory for electrical machines," *IEEE Transactions on Industrial Electronics*, Vol. 64, No. 8, 6063–6074, Aug. 2017.
3. Jahns, T. M., "Motion control with permanent-magnet AC machines," *IEEE Trans. Industry Applications*, Vol. 82, No. 8, 1241–1252, 1994.
4. Sneyers, B., D. W. Novotny, and T. A. Lipo, "Field weakening in buried permanent magnet AC motor drives," *IEEE Transactions on Industry Applications*, Vol. 21, No. 2, 398–407, 1985.
5. Chen, J., J. Li, et al., "Analysis, modeling, and current trajectory control of magnetization state manipulation in variable-flux permanent magnet machines," *IEEE Transactions on Industrial Electronics*, Vol. 66, No. 7, 5133–5143, 2018.
6. Jayarajan, R., N. Fernando, and I. U. Nutkani, "A review on variable flux machine technology: Topologies, control strategies and magnetic materials," *IEEE Access*, Vol. 7, 70141–70156, 2019.
7. Takaaki, I., N. Tsuyoshi, O. Sohei, et al., "Manufacturing and control of a variable magnetic flux motor prototype with a mechanical adjustment method," *Electrical Engineering in Japan*, Vol. 199, No. 1, 57–66, 2017.
8. Eiki, M., N. Noboru, and H. Katsuhiro, "Variable flux permanent magnet motor utilizing centrifugal force," *International Journal of Applied Electromagnetics and Mechanics*, Vol. 521, No. 2, 563–569, 2016.
9. Zhu, Z. Q., M. M. J. Al-Ani, X. Liu, et al., "A mechanical flux weakening method for switched flux permanent magnet machines," *IEEE Transactions on Energy Conversion*, Vol. 30, No. 2, 806–815, 2015.
10. Del Ferraro, L., F. Caricchi, et al., "Analysis and comparison of a speed-dependant and a torque-dependant mechanical device for wide constant power speed range in AFPM starter/alternators," *IEEE Transactions on Power Electronics*, Vol. 3, 720–729, 2006.
11. Liu, X., Y. Li, Z. Liu, et al., "Analysis and experimental investigation on flux-adjusting characteristic for a mechanical flux-adjusting axial PM synchronous machine," *Transactions of China Electrotechnical Society*, Vol. 33, No. 5, 9, 2018.
12. Liu, X., J. Xiao, H. Xu, et al., "Analysis of flux weakening performance of a novel variable flux permanent magnet synchronous machine with rotating magnetic pole," *Transactions of China Electrotechnical Society*, Vol. 35, No. 15, 9, 2020.
13. Liu, X., T. Sun, Y. Zou, et al., "Modelling and analysis of a novel mechanical-variable-flux IPM machine with rotatable magnetic poles," *IET Electric Power Applications*, Vol. 14, No. 4, 2020.
14. Cheng, S., C. Li, and B. Kou, "Research on the variable exciting function of a variable exciting magnetic reluctance PMSM," *Proceedings of the CSEE*, Vol. 27, No. 033, 17–21, 2007.
15. Chai, F. and Y. Bi, "Research review of flux-weakening methods of axial flux permanent magnet synchronous machine," *Micromotors*, Vol. 48, No. 02, 69–76, 2015.
16. Cao, Y., L. Feng, R. Mao, and K. Li, "Analysis of analytical magnetic field and flux regulation characteristics of axial-flux permanent magnet memory machine," *IEEE Transactions on Magnetics*, Early Access Article, 2022.
17. Ceylan, D., K. O. Boynov, and E. A. Lomonova, "Multi-objective optimization of a variable flux reluctance machine for high-torque operations," *2022 23rd International Conference on the Computation of Electromagnetic Fields (COMPUMAG)*, 1–4, 2022.
18. Liu, W., H. Yang, H. Lin, F. Peng, S. Lyu, and X. Huang, "Thermal modeling and analysis of hybrid-magnetic-circuit variable flux memory machine," *IEEE Transactions on Industry Applications*, 2022.